Depth-distributions and migration of fallout radionuclides in mountain soils from Chréa National Park (Algeria): The role of rhizospheres

Djamel Taieb Errahmani [a], Abdelkader Noureddine [a], José María Abril Hernández [b,*]

[a] Centre de Recherche Nucléaire d'Alger (CRNA), Commissariat à l'Energie Atomique. 02 Bd. Frantz Fanon, Box.399, Algiers, Algeria
[b] Departamento de Física Aplicada I, ETSIA, University of Seville, Spain

Keywords:

Fallout radionuclides

Mountain soils

Chréa park

Depth distribution

Rhizospheres

CDE models

A B S T R A C T

The distribution and migration of artificial fallout radionuclides in natural soils has been profusely studied for assessing radioecological impacts and predicting their long-term behaviour, among other topics. Despite the standardized use of the analytical solutions of a simplified convection-diffusion equation (CDE), there are still some concerns and open questions. This work is aimed at contributing to the understanding of basic processes governing the distribution of fallout radionuclides in vegetated soils with rhizospheres. It studies ^{210}Pb and ^{137}Cs in soil cores and vegetal samples from Chréa National Park, in Algeria, along with other natural radionuclides and some major and trace elements. Results include surficial and depth distributions of radionuclide concen-trations, and site and plant-specific concentration ratios (*CR*). Inventories of ^{137}Cs (3620 ± 120 Bq m^{-2}) and ^{210}Pb$_{exc}$ (9000 ± 900 Bq m^{-2}) in soils are typical from global fallout in high precipitation areas in the Northern Hemisphere. A simple model of a polyphasic soil, including rhizospheres, provides a realistic description in the studied case, where plant roots occupy about 45% of the volume in the 0–10 cm interval, with a high porosity around rhizomes. This composite soil matrix explains the different patterns observed in the depth distribution of the studied elements. The depth-distributions of ^{137}Cs and ^{210}Pb$_{exc}$ have been modelled with different ap-proaches: i) analytical solution of the CDE with mean annual convection and large observation times; ii) as before, but with convection representing infiltration events and short observation times; iii) numerical modelling of the ^{137}Cs profile in the mineral phase using CDE with fast initial distributions. The three approaches fit the empirical data, but they predict different time evolutions. The approach iii) provides a more realistic description. Results are questioning the common accepted analysis and its predictive use.

1. Introduction

The distribution and migration of artificial fallout radionuclides in natural soils have been profusely studied topics in the scientific literature after the nuclear weapon tests carried out in the 50's and early 60's in the past century. The number of studies sharply increased following the major nuclear accidents of Chernobyl (1986) and Fukushima (2011). These studies are relevant, among other topics, for predicting their long-term behaviour in the environment, assessing radioecological impacts due to their uptake by plants and fauna, including human food chains, and for designing remediation actions. Most of the studies have focused on ^{137}Cs, ^{134}Cs and ^{90}Sr; and, although with less coverage, on $^{239+240}$Pu, ^{241}Am and ^{60}Co, among others (e.g., Knatko et al., 1996; Smith et al., 1997; IAEA, 2010; Ni et al., 2018; Liu et al., 2021).

Lead-210 is a natural-occurring radionuclide from the ^{238}U series. In the atmosphere, it is generated by the radioactive decay of the ^{222}Rn exhaled by the continental crust. After dry and wet deposition, it is found in the upper soil layers as the fraction in excess (labelled ^{210}Pb$_{exc}$ hereafter) with respect to the ^{210}Pb originated from the in-situ decay chain of ^{226}Ra. This isotope is often included along with the above radionuclides to get further insights on the basic processes and parameter values involved in their migration in soils (e.g., He and Walling, 1997; Itthipoonthanakorn et al., 2019). As an interesting application, it is worth mentioning that the comparative study of ^{210}Pb$_{exc}$ and ^{137}Cs inventories in natural and agriculture soils with respect to reference sites can support the assessment of soil erosion (see the review by Mabit et al., 2014).

The soil is a heterogeneous, polyphasic (solid, liquid and gaseous),

Abbreviations: CDE, convection-diffusion equation.

* Corresponding author.
E-mail address: jmabril@us.es (J.M. Abril Hernández).

particulate, disperse, and porous system, with large interfacial areas (Hillel, 1971). Radionuclides can be found in the soil solution (liquid phase) or bound to solids, in both reversibly adsorbed and fixed fractions. It is widely accepted that the basic abiotic processes controlling mobility of radionuclides in undisturbed soils include convective and diffusive transport in the pore fluid and physic-chemical interaction with the soil matrix (Kirchner et al., 2009; IAEA 2010). This is often described by a simplified convection-diffusion equation (CDE). Thus, it is assumed an instantaneous, reversible and concentration independent partitioning between solid and liquid phases, and uniform and constant values for soil porosity, effective dispersion coefficient, D, and convective velocity, v. When, in addition, the input of radionuclides into the soil is described by a pulse-like function ($J_o\delta(t)$, with J_o being the deposition density or inventory, in Bq m^{-2}), it is possible to find out an analytical solution for their volumetric concentrations in the soil, $C(x,t)$, as a function of depth, x, and time, t (Bossew and Kirchner, 2004; Legarda et al., 2011):

$$C(x,t) = J_o e^{-\lambda t}\left\{\frac{1}{\sqrt{\pi D t}} e^{-(x-vt)^2/(4Dt)} - \frac{v}{2D} e^{vx/D} erfc\left(\frac{v}{2}\sqrt{\frac{t}{D}} + \frac{x}{2\sqrt{Dt}}\right)\right\} \quad (1)$$

In Eq. (1) λ is the radioactive decay constant of the studied radionuclide. The effective dispersion coefficient relates to the physical dispersion coefficient, D' (molecular diffusion and hydrodynamic dispersion), through the retardation factor, R_d: $D = D'/R_d$. This last relates with the solid/liquid partition coefficient, k_d, the soil porosity, φ, and its bulk density, ρ_b (Kirchner et al., 2009): $R_d = 1 + \frac{\rho_b}{\varphi} k_d$. Similarly, the effective convective velocity relates with the mean pore-water velocity, v_w as $v = v_w/R_d$. The compilation of a huge amount of literature data about vertical migration of radionuclides in undisturbed meadow soils (agricultural and semi-natural) has allowed for reporting reference values and ranges for D and v as a function of the soil type according to texture and organic matter content (IAEA, 2010). The mathematical properties of the analytical solution of Eq. (1) have been discussed in Bossew and Kirchner (2004). A potentially important limitation is its failure to describe "young'' profiles shortly after fallout.

Other approach used in the scientific literature for studying radionuclide depth-profiles in soils consists in fitting the data to simple analytical functions such as Gaussians, exponentials, or hyperbolic secant functions. This allows estimating some descriptive parameters (e.g., Matsuda et al., 2015). Other works have used multi-compartmental models as discrete analogues of the CDE (e.g., Kirchner, 1998). A comprehensive review and application of different analytical and compartmental models can be seen in Mishra et al. (2016).

The study of radionuclide distribution in soils is far of being a closed problem. It is true that Eq. (1) in most cases produces good fits for a single time of observation. Moreover, for ^{137}Cs, the order of magnitude of v is of ~0.3 cma^{-1}, while k_d is ~10^3, what leads to v' values of the order of magnitude of the annual rainfall rate, what seems to be self-consistent. However, when studying a temporal sequence of soil cores the fitted values for the migration velocity often decrease with time (see discussion of this point in Chaif et al., 2021).

Novel models have been suggested explicitly including non-equilibrium sorption on the vertical migration of ^{137}Cs. Kurikami et al. (2017) coupled the CDE with kinetic reversible/irreversible sorption terms to model ^{137}Cs soil profiles in Fukushima Prefecture. Similarly, Chaif et al. (2021) distinguished two reaction sites in solids: type-1 sites being governed by instantaneous linear and reversible sorption, and type-2 sites with kinetically controlled first-order sorption with constant rates. Nevertheless, the above works still used the annually or the monthly-averaged infiltration rates in the convective term. This approach disagrees with the wide empirical evidence of a fast initial depth-distribution of radionuclides in soils. Thus, Schimmack et al. (1989) studied the vertical distribution of Cs isotopes in soils sampled shortly after receiving the Chernobyl fallout. They observed rates of migration between 0.2 and 0.3 cm h^{-1}, being considerably faster than the values estimated in the same soils for the long-term migration of ^{137}Cs from the global fallout of weapon-testing (0.4–1.0 cm a^{-1}).

It seems more realistic considering fast initial distributions of fallout radionuclides in soils following wet deposition. Such distributions would be governed by the instantaneous infiltration rates (of the order of few cm h^{-1} – Hillel, 1971) and the uptake kinetics, which can be described by a set of parallel and/or consecutive first-order reactions (Barros and Abril, 2005, 2008). The global depth- profiles of fallout radionuclides in the soil could be seen then as the aggregate result of many depositional events composing the fallout history. Nevertheless, there is also wide empirical evidence of that those depth-profiles still undergo changes over time (Schimmack and Schultz, 2006).

He and Walling (1997) suggested that the primary factors influencing the post-depositional redistribution of these radionuclides in stable undisturbed soils could be represented as effective diffusion and convection processes. Thus, they solved a CDE imposing as initial conditions an exponential depth distribution instead of the classical initial condition of a clean soil. The boundary conditions did not included any further fluxes of radionuclides at the soil surface. Mishra et al. (2016) presented analytical solutions for a modified CDE model, in which an exponential profile is assumed as initial condition, resulting from fast infiltration. They included further modifications by considering a fixed or non-exchangeable phase, and a simple kinetic sorption model. This approach was also considered by Abril and Gharbi (2012) to explain the co-occurrence of fast and slow redistribution processes of fallout radionuclides in aquatic sediments. The former were described as a depth-distributed source term in the CDE, along with the consistent update of the boundary conditions. This allowed for solving the depth profiles arising as the aggregate result of the whole fallout history instead of a single depositional event.

Concerns on the use of Eq. (1) also arise from the implicit assumption of uniform soil properties. As it will be shown in this paper, the observed structure of the depth profile of volumetric concentrations can be partially contributed by low values of bulk density at the upper soil, what can lead to misestimating the apparent migration rates.

A more profound concern is the role of rhizospheres in vegetated soils, which is ignored in all the above versions of the CDE. Ehlken and Kirchner (2002) presented a detailed discussion on the basic processes involving the rhizospheres, and affecting radionuclide mobility and their partitioning in soils. Two major effects of rhizospheres can be considered concerning the CDE: i) their role in conforming the soil structure through which the porewater flows; ii) they conform a distinct soil-phase with a differential behaviour for the uptake, partitioning and mobility of radionuclides.

In most cases, rhizospheres hardly can be separated from the mineral soil, and the bulk sample is processed. The water content determined by gravimetric methods after oven drying does not only represent the pore fluid, but also the water in vegetal-tissues. Plant roots occupy part of the soil volume, and thus diminishing the pore space available for free-water and air, and for the convective transport and kinetic uptake by mineral solids during infiltration events.

The concentration in vegetal tissues (in a dry weight basis) for most radionuclides is typically lower than in the bulk soil (IAEA 2004, 2010). As result, measuring radionuclide concentrations in bulk soil samples can mask the singular fingerprints of their sorption and distribution within the mineral phase (Iurian et al., 2021), leading then to misinterpretations of parameters describing the mobility and fate of radionuclides in soils.

This paper is aimed at contributing to the understanding of basic processes governing the depth-distribution of fallout radionuclides in vegetated soils with well-defined rhizospheres. It is based upon field studies with soil cores sampled in the Chréa National Park, in Algeria. Target radionuclides are the naturally occurring ^{210}Pb and the ^{137}Cs from the atmospheric nuclear weapon tests. The study comprises a high-resolution soil core (sliced at 1–2 cm intervals), complemented with a set of low-resolution cores (sliced at a minimum of 5 cm intervals), samples

of surficial soils (0–5 cm depth), and vegetal tissues (roots and aerial parts of the natural grass cover). Analytical methods included other natural gamma emitting radionuclides and the physical and chemical characterization of the soil, accounting for its water content, bulk density, organic matter (OM), porosity, and rhizosphere volume (as estimated by a polyphasic model of the soil).

The present work is also aimed at complementing the field data existing until date in Algeria on ^{137}Cs and ^{210}Pb concentrations in soils and plants. Among relevant previous works, it is worth mentioning the national environmental sampling program for reporting levels of natural and artificial radionuclides in the 0–15 cm soil layer in Algeria (Baggoura et al., 1998), and the study of ^{137}Cs depth profiles in semi-arid land of western Algeria for soil erosion assessment (Azbouche et al., 2017). Also mentioning the reports on gamma emitting radionuclides in soil cores and surficial soils samples (Nadri et al., 2019a, 2019b).

2. Materials and methods

2.1. The study site, sampling and sample treatment

The Chréa National Park is located 50 km south-west of the capital Algiers, along the northern and southern ridges of the Blida section of the Atlas Mountains. Founded in 1997, it is one of the largest national parks in Algeria, with an area of 36,985 ha. The park is a Biosphere Reserve; it hosts 1210 plant and animal species, such as the Atlas cedar (*Cedrus atlantica*) and the monkey *Macaca Sylvanus* (UNESCO, 2021). This Park plays a vital role as a water reservoir for large cities like Algiers, Blida and Médéa. The area is characterized by a cool Mediterranean climate, with an average annual rainfall ranging from about 700 mm at Blida to about 1400 mm on the top of the mountain. The summer is generally hot and dry and the winter is cold and wet with snowfall.

Surficial soils, low and high-resolution soil cores, and vegetal tissues (roots and aerial parts) were sampled at different sites and times, as summarized in Table 1 and Fig. 1. For low-resolution cores, the subsamples after sectioning (see Table 1) will be labelled hereafter with subindexes 1,2… following increasing depths. For vegetal samples, subindexes R and AP will be used for referring to roots and aerial parts, respectively. The sampling strategy fits the stated aims: i) studying basic processes on fallout-radionuclide distribution in vegetated soils; ii) complementing the field data existing until date in Algeria on ^{137}Cs and ^{210}Pb concentrations in soils and plants. The high-resolution core fits aim i), and low-resolution cores serve for comparison. These latest, along with the remaining samples fit aim ii). The set allows for determining site and plant specific concentration ratios, which are useful for describing the polyphasic soil environment involved in aim i).

Sampling points were in clear areas within the forest, sufficiently apart from trees, and with a low vegetal cover, consisting mostly on grass (see Fig. S1, in electronic supplementary material, ESM). Their selection obeys to a reasonable compromise between representativeness and practicability. Topographical slopes for these undisturbed mountain soils were not measured. The geographical coordinates and elevations were determined using a GPS device.

Surface soils (0–5 cm depth) were sampled in the corners and the centre of a 1m-side square using an appropriate shovel, and after removing the aerial part of the vegetal cover. These subsamples were mixed to get a homogeneous representative sample of about 1 kg. The lack of control of bulk volumes does not allow estimating bulk densities and inventories, but they are useful for comparison of their radionuclide concentrations, and for estimation of plant concentration ratios (see below).

Soil cores were sampled by using a manual corer manufactured with a metallic pipe, covering a Plexiglas tube inside, of 9.5 cm inner diameter. The corer was introduced into the soil using a hammer. Then it was retired to recover and protect with caps the sample inside the Plexiglas cylinder. The sampling depths with this procedure ranged from 10 to 37 cm (see Table 1). For sampling the high-resolution core (S4), of 41 cm length, the soil was previously wetted by excavating a 0.5 m-side squared perimeter, which was filled with water until apparent saturation (see details in Fig. S2, in ESM).

Table 1
Sampling sites and sample description: Soils (S) and plants (P) from the Chréa National Park.

Code	Location	Date	Elevation (m)	Sampling depth (cm)	Slicing intervals (cm)
S1	36°25.88′N, 2°53.08′E	31/03/2016	1500	10	(0–5), (5–10)
S2	36°27.21′N, 2°51.75′E	31/03/2016	900	5	(0–5)
S3	36°28.07′N, 2°51.30′E	04/05/2016	600	5	(0–5)
S4	36°25.90′N, 2°53.03′E	24/04/2017	1518	41	1 cm in (0–5); 2 cm in (5–41)
S5	36°26.06′N, 2°52.65′E	07/07/2020	1282	20	(0–10), (10–20)
S6	36°26.44′N, 2°52.24′E	07/07/2020	1218	32.5	(0–12), (12–22), (22–32.5)
S7	36°26.84′N, 2°51.97′E	07/07/2020	1041	37	(0–7), (7–17), (17–27), (27–37)
S8	36°27.69′N, 2°51.38′E	07/07/2020	713	25	(0–5), (5–15), (15–25)
S9	36°25.91′N, 2°53.03′E	25/04/2021	1511	5	(0–5)
S10	36°26.65′N, 2°54.03′E	25/04/2021	1434	5	(0–5)
S11	36°26.85′N, 2°54.34′E	25/04/2021	1035	5	(0–5)
S12	36°27.58′N, 2°51.58′E	25/04/2021	730	5	(0–5)
P9	36°25.91′N, 2°53,03′E	25/04/2021	1511	–	Roots, aerial parts
P10	36°26.65′N, 2°54.03′E	25/04/2021	1434	–	Roots, aerial parts
P11	36°26.85′N, 2°54.34′E	25/04/2021	1035	–	Roots, aerial parts
P12	36°27.58′N, 2°51.58′E	25/04/2021	730	–	Roots, aerial parts

In the sampling campaign of 2021, samples of surficial soils, roots and aerial part of plants were collected at each sampling point. Vegetal samples are denoted with the same number than soils. S4, sliced at 1–2 cm intervals, is referred in the text as high-resolution core; surficial soils correspond to 0–5 cm depth; the remaining soil samples are referred as low-resolution cores.

The soil cores were sectioned at the laboratory (see details in Table 1). The samples were preserved in plastic containers until oven drying at 70 °C to constant weight. Some small stones were found in surficial samples of cores S5 to S8. They were removed before proceeding with the sample treatment. The dried samples were ground to fine powder by using a centrifugal grinder Retsch S100, sieved on a 2 mm mesh, and homogenized before analysis. The water content in each soil slice was estimated from the wet and dry weights, while bulk densities were determined by the ratio between dry weight and the known volume for each slice. Loss on ignition (LOI) analysis were used as a proxy for estimating the organic matter content (% OM) of soil samples. Two grams of the dried samples were ignited at 480 °C for 4 h (Luczak

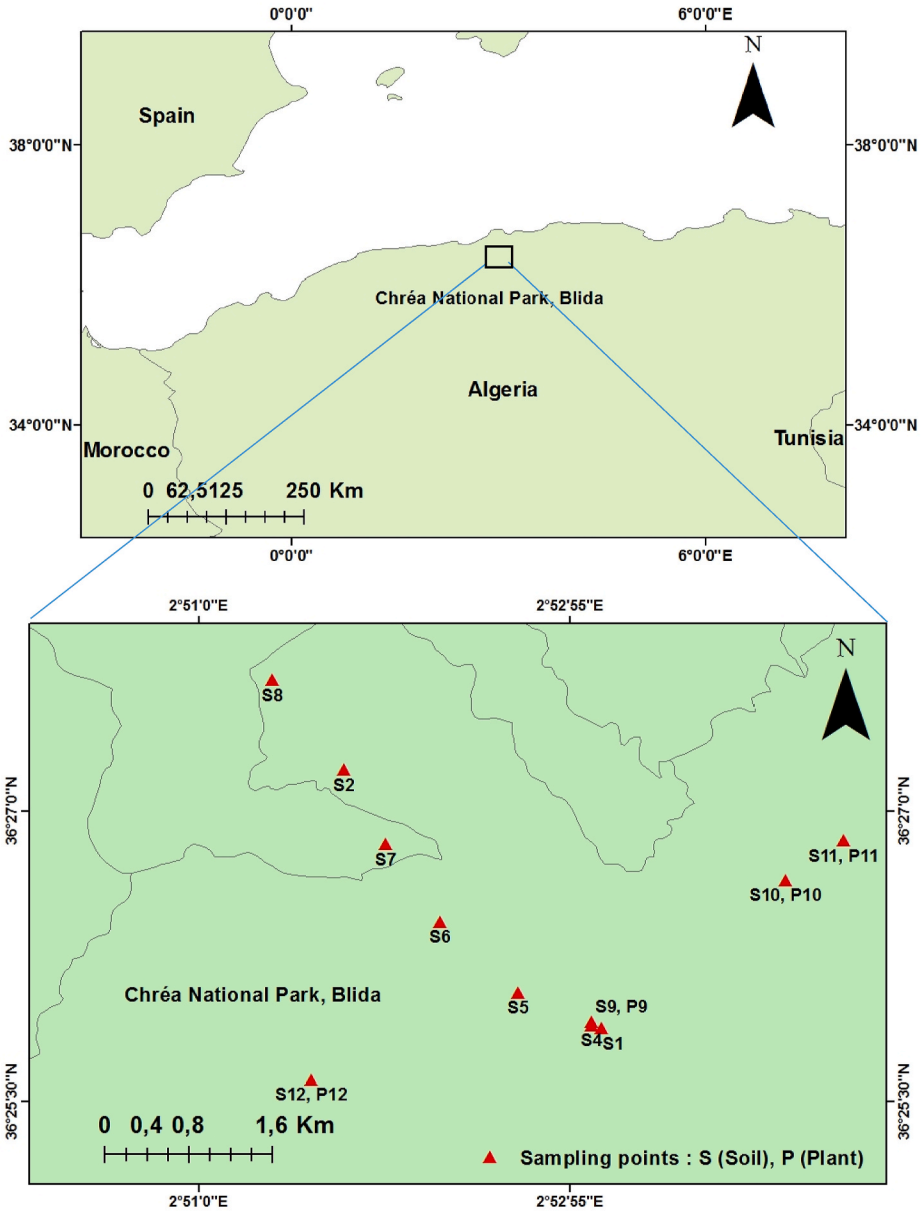

Fig. 1. Map with the sampling sites for soils (S1 to S12) and plant tissues (P9 to P12) in the Chréa National Park, Algeria.

et al., 1997).

At sites 9 to 12, the aerial part of the vegetal cover was cut and recovered before the sampling of surficial soils. Adjacent areas of c.a. 1 m^2 were sampled in the same way until getting a total mass of about 1 kg. In the same adjacent areas, the surficial soil was removed, and macro roots were collected with minimum amounts of soil adhered. In the laboratory, vegetal samples were oven dried at 70 °C to constant weight. In the samples of plant roots, the remaining mineral soil particles were removed as much as possible. After that, all the vegetal samples were cut into small pieces and ground. Measurements of fresh and dried weights allowed for the determination of the water content in the organic samples. This ranged from 69% to 76% in plant roots, and from 34% to 51% in the aerial parts. The dominant plant species were *Poa pratensis* L. in sites S9 to S11 and *A. mauritanicus* – A. in site S12.

Prior the gamma measurements, about 100 g of soil and vegetal samples were sealed in cylindrical plastic containers of 100 cm^3 and 250 cm^3, respectively, to avoid ^{222}Rn scape, and they stored for a period of at least three weeks to ensure secular equilibrium among ^{226}Ra and its progeny radionuclide ^{214}Pb.

2.2. Chemical composition

Major and trace elements in soil samples from selected depths in core S4 were analyzed by Wavelength –Dispersive X-Ray Fluorescence Spectrometer (WDXRF), using a Panalytical Philips Magix Pro and PW2440 model. Two grams of each soil sample were prepared as pressed pellets using a licowax binder at a pressure of 18 tons and measured for 24.5 min. The calibration was done with the Omnian standardless analysis software by using a set of reference samples delivered by PANalytical. The detection limit (within brackets) varied from an element to another: C (9 ppm), Al (11.5 ppm), Si (1.1 ppm), P (1.9 ppm), Fe (1.2 ppm), Rb (1.8 ppm) and Sr (3.8 ppm). Uncertainties ranged from 1.9 to 10.5%.

2.3. Gamma spectrometry analysis

Gamma spectrometry measurements were performed to determine ^{210}Pb, ^{212}Pb, ^{214}Pb, ^{137}Cs, ^{228}Ac and ^{40}K activities using a coaxial High purity Germanium (HPGe) detector with a 40% of relative efficiency (a

GX4018 from Canberra), and Genie-2000 software. Measurements were carried out at the Centre de Recherche Nucléaire d'Alger (CRNA). Typical counting times ranged from 24 to 48 h. Mass activity concentrations of ^{226}Ra were estimated through its progeny radionuclide ^{214}Pb. For radionuclides from the ^{232}Th series, ^{228}Ra was estimated through ^{228}Ac, and ^{228}Th through ^{212}Pb. Unsupported ^{210}Pb activity concentrations were determined for each slice by subtracting the activity concentrations of ^{226}Ra from the total ^{210}Pb activity concentrations. The energies considered for the activity calculations were: 46.5 keV for ^{210}Pb, 238.6 keV for ^{212}Pb, 351.9 keV for ^{214}Pb, 661.6 keV for ^{137}Cs, 911.2 keV for ^{228}Ac and 1460.8 keV for ^{40}K.

Energy and resolution calibrations were determined using point sources of ^{241}Am, ^{137}Cs and ^{60}Co. The detector efficiency was calibrated as described in Taieb Errahmani et al. (2020). In–house calibration sources were prepared by spiking soil samples with liquid sources of ^{152}Eu and ^{133}Ba. EFFTRAN software (Vidmar, 2005) was used for true-coincidence summing and self-absorption corrections. Standards with a range of masses were prepared with the same geometry as the samples. As reported in the above reference, the analytical procedure was checked using the proficiency test soil sample IAEA TEL 2018 (natural soil spiked with anthropogenic gamma emitter radionuclides). For organic samples, we used the CRM IAEA –330 (spinach) and CRM IAEA 447 (Moss Soil) as calibration standards.

2.4. Models for radionuclide distribution in soils

This work uses the simplified CDE for volumetric concentrations, as formulated by Bossew and Kirchner (2004). Eq. (1) gives its analytical solution for pulsed inputs, and it is routinely applied for ^{137}Cs profiles.

The same approach of a simplified CDE can be applied to ^{210}Pb$_{exc}$. The effective dispersion coefficient, D, and convective velocity, v, take different values than for ^{137}Cs, due to the different k_d values involved in the retardation factor. As boundary condition, a constant flux, F, must be considered instead of a pulsed input. The steady state solution for this problem, in terms of volumetric concentrations, is:

$$C(x) = \frac{F}{v - D\beta} e^{\beta x} \; ; \; \beta = \frac{v - \sqrt{v^2 - 4\lambda D}}{2D} \tag{2}$$

In Eq. (2) λ is now the radioactive decay constant for ^{210}Pb.

We adopted the formulation by Abril and Gharbi (2012) for modelling fallout histories at decadal or centennial scales as the aggregate result of fast initial depth-distributions, followed by tiny post-depositional redistribution. This last process is approached as an effective convection-diffusion. The model is presented in detail in section 3.5, after completing the view on the involved magnitudes and processes.

2.5. A polyphasic model of the soil matrix accounting for rhizospheres

Fig. 2 shows a sketch for supporting the concept presentation. Stacked solids and plant roots conform the structure of the porous medium, with the pore spaces partially occupied by water. In terms of partial volumes, the soil can be seen as being composed of i) mineral particles; ii) detrital organic matter; iii) vegetal tissues conforming the rhizosphere (this includes tissue water); iv) pore fluid, with dissolved salts; v) air pores. In terms of masses, there are three components: inorganic, organic, and pore fluid. The mass of the gaseous phase is negligible.

From a non-saturated bulk soil sample of known volume, V_b, and a wet mass m_{wet}, its water content can be determined by a gravimetric method after oven-drying till constant weight, m_{dry}, and it can be expressed as the ratio $f_w = (m_{wet} - m_{dry})/m_{wet}$. This includes the pore and the tissue waters.

The organic matter in the dry fraction of the soil can be determined by the LOI method, what includes both the initially detrital and the former rhizosphere components. When corrections by the salinity of the pore fluid are neglected, the bulk density of the soil is $\rho_b = m_{dry}/V_b$. The mass of organic matter is $m_{org} = f_{org} m_{dry}$, where f_{org} is the LOI percentage, but expressed as a fraction. The mineral bulk density can be defined as $\rho_{b,\,min} = m_{min}/V_b = (1\text{-}f_{org})\rho_b$.

Without further physical separation, the masses for the other components of the soil only can be determined after gross approaches. At depths below the rhizosphere, only the detrital fraction of the organic matter is present. As a crude simplification, the baseline values found below the rhizosphere, $f_{org,D}$, can be assumed as being uniform in the entire soil core. This allows estimating the component of the organic matter in the rhizosphere: $m_{org,T} = (f_{org} - f_{org,D}) m_{dry}$.

The fraction of dry mass in fresh vegetal tissues can be empirically determined (e.g., see Table 62 in IAEA, 2010). A uniform value will be adopted here, and labelled as f_T. The mass of fresh vegetal tissue is then $m_{org,T}/f_T$, and the mass of tissue water is $m_{w,T} = m_{org,T}(1 - f_T)/f_T$. Finally, the mass of pore water is $m_{w,P} = m_{wet} - m_{dry} - m_{w,T}$.

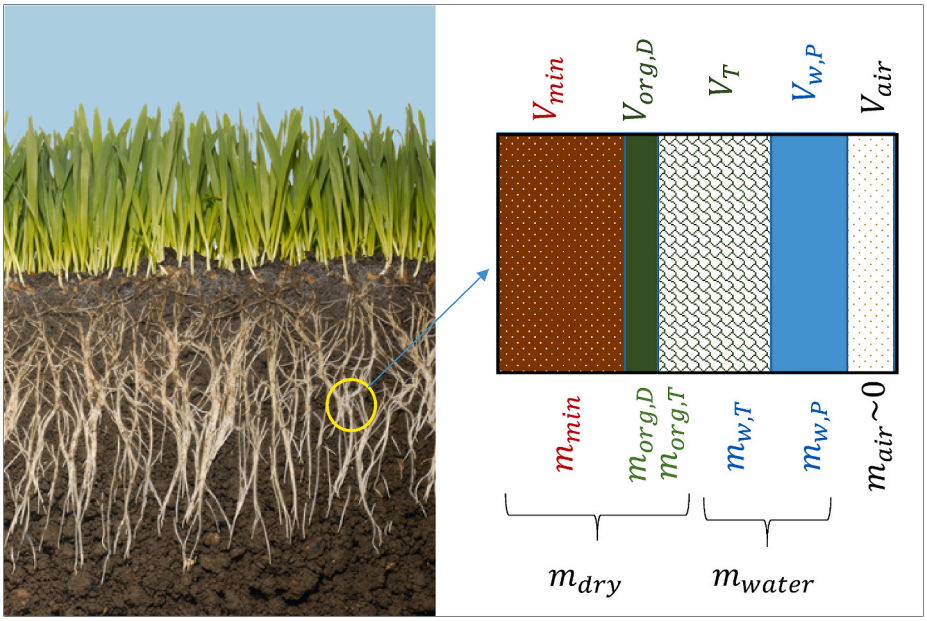

Fig. 2. Sketch for a polyphasic model of the upper soil, including rhizospheres. In terms of volume, it is composed of mineral soil (V_{min}), detrital OM ($V_{org,\,D}$), tissue of plant roots (V_T), and pore spaces partially occupied by water (V_{wP}) and air (V_{air}). After oven drying at constant weight (m_{dry}), tissue water ($m_{w,T}$) and pore water ($m_{w,P}$) disappear, and the detrital ($m_{org,D}$) and former living OM ($m_{org,T}$) conform a single analytical phase (m_{org}). With standard analytical procedures and a series of assumptions, it is possible to get reasonable proxies to the polyphasic state of the soil at the time of slicing.

Once the masses of the different components of the soil have been estimated within a known volume, it is possible handling typical values of their densities (e.g., 2.5, ~1.3, ~1.1 and 1.0 g cm^{-3} for mineral soil, organic detrital, vegetal tissue and pore water, respectively) for getting their respective volume fractions. The remaining amount to complete the total known volume corresponds to the air pores.

The porosity of the soil in the studied volume is $\varphi = \left(\frac{m_{w,P}}{\rho_w} + V_{air}\right) \Big/ V_b$, where ρ_w is the density of porewater. The porosity is a function of depth. It is possible defining the fraction of the porosity occupied by pore water as $\varepsilon = 1/\left(1 + \frac{V_{air}\ \rho_w}{m_{w,P}}\right)$.

2.6. Concentration ratios (CR)

The transfer factor (concentration ratio) for the uptake of any radionuclide from soil to plant is defined as the ratio of the dry weight concentration in the plants to the dry weight concentration in the specified soil layer (IAEA, 2010). In practice, this concept becomes an operational definition. Thus, instead of the real rooting depth, a standardized soil layer is adopted. In this work we used the 0–5 cm soil layer, where radionuclide concentrations were determined in the bulk soil samples without separation of plant roots. The choice of the soil layer is particularly relevant for those radionuclides with non-uniform depth distributions, such as fallout radionuclides.

This work estimates concentration ratios for roots and the aerial part of plants. While the later can be well separated at the soil surface level, the former must be manually disaggregated from the inorganic solids, what always results in some degree of mineral-remains in the sample.

3. Results and discussion

3.1. The empirical dataset

Table 2 summarizes results for the high-resolution core S4, including water content, OM, bulk density, and radionuclide activity concentrations for each slice. Results from the measurements in the other soils appear in Table 3. The measurements of the organic samples and the estimation of radionuclide concentration ratios are reported in Table 4. Table S1 (ESM) reports the WDXRF analysis of major and trace elements in soil samples from selected depths in core S4.

The activity-concentration ratio $^{228}Ra/^{212}Pb$ informs on the secular equilibrium within the ^{232}Th series. In core S4 this ratio is 0.99 ± 0.03 (mean and standard deviation of the mean). For soils S5 to S12 this ratio takes the value 1.00 ± 0.01, indicating secular equilibrium between ^{228}Ra and ^{228}Th.

The activity-concentration ratio $^{228}Ra/^{226}Ra$ informs on the relative proportion of the natural radioactive decay series of ^{232}Th and ^{238}U. In core S4, this ratio is 1.58 ± 0.03 (mean and standard deviation of the mean). For soils S5 to S12, this ratio takes the value 1.75 ± 0.03. In the continental crust the $^{232}Th/^{238}U$ mass ratio converge on a value of around 5 or slightly higher (Paul et al., 2003), what corresponds to an activity-concentration ratio of ~1.6. Present results are in very good agreement with the above figure (of ~1.6), and they compare well with the activity-concentration ratios $^{232}Th/^{226}Ra$ reported by Mehra and Singh (2011) for soils of different geological origin in northern India.

The measured activity concentrations of ^{212}Pb, ^{226}Ra and ^{40}K in soils S4 to S12 are well in the range of typical values in soils, and particularly within the values reported for a wide survey of soils in Algeria (Baggoura et al., 1998).

In soil core S4, the artificial ^{137}Cs was found up to a depth of 20 cm. For the slice of index i, with bulk density $\rho_{b,i}$ and thickness Δx_i, the measured activity concentration is denoted as A_i, and the inventory in this slice is $\Delta\Sigma_i = \rho_{b,i}\Delta x_i A_i$.The cumulative inventory at a certain depth x_j, is obtained by summing the contributions of all the slices above x_j.

Fig. 3 shows the cumulative inventories as a function of depth for the soil cores S4 to S8. They asymptotically increase until a constant value, which is the total inventory. Penetration depths are roughly of 20 cm depth (slightly higher in core S8).

Table 5 reports the total inventories of ^{137}Cs referred to a common date (July 7th, 2020). The total $^{210}Pb_{exc}$ inventories were estimated as in the case of ^{137}Cs. Negative values of $^{210}Pb_{exc}$ were not considered for inventories. This point will be discussed in more detail further below. Results are included in Table 5. The $^{210}Pb_{exc}$ inventory is these soils, Σ_{Pb}, is assumed to be steady state, so the equivalent constant $^{210}Pb_{exc}$ flux can be estimated as $F_{Pb} = \lambda_{Pb}\Sigma_{Pb}$, where λ_{Pb} is the radioactive decay constant

Table 2
Physical parameter and activity concentrations (Bq.Kg^{-1}) of natural and artificial radionuclides in the soil core S4 at Chréa mountain.

Depth	f_w	f_{org}	ρ_b	^{137}Cs	^{210}Pb	^{212}Pb	^{226}Ra	^{228}Ra	^{40}K
(cm)			(g cm^{-3})	(Bq kg^{-1})					
0.5	0.64	0.48							
1.5	0.62	0.48	0.33	35 ± 3	281 ± 50	26 ± 5	12.5 ± 2.7	25 ± 7	310 ± 30
2.5	0.59	0.35	0.30	41 ± 4	283 ± 55	27 ± 5	17 ± 3	24 ± 7	340 ± 40
3.5	0.55	0.41	0.39	46 ± 4	242 ± 50	28 ± 5	17 ± 3	23 ± 6	390 ± 40
4.5	0.52	0.36	0.55	42 ± 4	190 ± 40	31 ± 6	16 ± 3	25 ± 6	400 ± 40
6	0.44	0.27	0.73	50 ± 4	170 ± 30	40 ± 8	19 ± 4	33 ± 8	540 ± 60
8	0.39	0.23	0.77	47 ± 4	117 ± 23	44 ± 8	24 ± 5	37 ± 9	630 ± 70
10	0.30	0.15	1.16	32 ± 3	78 ± 15	50 ± 10	26 ± 5	43 ± 11	730 ± 80
12	0.24	0.08	1.24	13.9 ± 1.2	39 ± 8	40 ± 8	29 ± 6	45 ± 11	740 ± 80
14	0.20	0.07	1.46	6.8 ± 0.6	22 ± 5	40 ± 8	31 ± 6	48 ± 12	790 ± 80
16	0.18	0.07	1.60	3.8 ± 0.3	15 ± 3	53 ± 10	31 ± 6	49 ± 12	790 ± 80
18	0.17	0.06	1.78	2.92 ± 0.26	8.5 ± 2.4	57 ± 11	31 ± 6	50 ± 12	820 ± 90
20	0.16	0.07	1.46	1.27 ± 0.12	7.2 ± 2.5	58 ± 11	30 ± 6	47 ± 12	810 ± 90
22	0.16	0.06	1.42	–	15 ± 3	55 ± 11	28 ± 5	47 ± 12	800 ± 80
24	0.16	0.08	1.07	–	16 ± 3	55 ± 11	29 ± 6	47 ± 12	780 ± 80
26	0.15	0.05	1.69	–	10.4 ± 2.8	43 ± 8	34 ± 6	51 ± 13	840 ± 90
28	0.15	0.06	1.77	–	20 ± 5	45 ± 9	37 ± 7	53 ± 13	860 ± 90
30	0.15	0.05	1.66	–	20 ± 5	45 ± 9	34 ± 7	51 ± 13	860 ± 90
32	0.14	0.05	2.13	–	24 ± 5	48 ± 9	35 ± 7	53 ± 13	860 ± 90
34	0.14	0.05	1.52	–	16 ± 4	46 ± 9	32 ± 6	53 ± 13	870 ± 90
36	0.14	0.05	1.80	–	18 ± 4	44 ± 8	32 ± 6	49 ± 12	840 ± 90
38	0.14	0.05	1.32	–	20 ± 4	43 ± 8	31 ± 6	49 ± 12	820 ± 90
40	0.12	0.05	1.72	–	17 ± 4	43 ± 8	31 ± 6	48 ± 12	810 ± 90

f_w is the water content at slicing (fraction), f_{org} is the fraction of organic matter in the oven-dried sample, and ρ_b is the dry bulk density.
^{226}Ra is determined through ^{214}Pb. N.M. not measured. Because the low mass, the 0–1 cm section was not measured for gamma analysis.
Radionuclide activity concentrations refer to the date of sampling (Table 1).

Table 3
Physical parameter and activity concentrations ($Bq.Kg^{-1}$) of natural and artificial radionuclides in the soils at Chréa mountain.

Sample	Depth	f_{org}	ρ_b	^{137}Cs	^{210}Pb	^{212}Pb	^{226}Ra	^{228}Ra	^{40}K
	(cm)		(g cm^{-3})	(Bq kg^{-1})					
$S1_1$	0–5	N.M.	N.M.	42.6 ± 2.2	N.M.	N.M.	N.M.	N.M.	N.M.
$S1_2$	5–10	N.M.	N.M.	56.7 ± 2.9	N.M.	N.M.	N.M.	N.M.	N.M.
S2	0–5	N.M.	N.M.	11.0 ± 0.6	N.M.	N.M.	N.M.	N.M.	N.M.
S3	0–5	N.M.	N.M.	19.4 ± 1.0	N.M.	N.M.	N.M.	N.M.	N.M.
$S5_1$	0–10	0.20	0.93	50.3 ± 2.6	158 ± 10	43.8 ± 2.5	24.9 ± 1.6	44 ± 3	660 ± 30
$S5_2$	10–20	0.09	1.47	8.3 ± 0.5	25.4 ± 2.7	50.9 ± 3	29.1 ± 1.6	52 ± 3	780 ± 30
$S6_1$	0–12	0.19	1.25	32.0 ± 1.7	61 ± 5	42 ± 3	24.6 ± 1.6	43 ± 3	544 ± 25
$S6_2$	12–22	0.09	1.66	1.2 ± 0.3	25 ± 3	44.5 ± 2.2	25.0 ± 1.6	46 ± 3	525 ± 26
$S6_3$	22–32	0.14	1.39	N.D.	26 ± 3	48.8 ± 2.5	29.5 ± 1.7	52 ± 3	577 ± 27
$S7_1$	0–7	0.09	1.51	42.7 ± 2.4	80 ± 6	49 ± 3	25.6 ± 2.7	52 ± 3	525 ± 25
$S7_2$	7–17	0.07	1.65	8.8 ± 0.7	41 ± 4	55 ± 3	31.0 ± 1.8	56 ± 4	571 ± 27
$S7_3$	17–27	0.08	0.92	0.8 ± 0.3	26 ± 3	57 ± 4	32.2 ± 1.9	57 ± 4	569 ± 26
$S7_4$	27–37	0.09	0.92	0.5 ± 0.2	17 ± 3	57 ± 3	31.6 ± 1.6	55 ± 3	488 ± 22
$S8_1$	0–5	0.18	1.48	54.4 ± 0.8	143 ± 9	32.2 ± 1.6	18.1 ± 1.3	31.5 ± 2.6	444 ± 23
$S8_2$	5–15	0.09	1.16	43.4 ± 2.2	63 ± 4	45 ± 3	26.6 ± 1.4	45.4 ± 2.6	603 ± 28
$S8_3$	15–25	0.08	1.01	23.8 ± 1.3	41 ± 4	46 ± 4	28.4 ± 2.0	49 ± 3	640 ± 30
S9	0–5	0.47	N.M.	101 ± 6	414 ± 26	33.0 ± 2.5	22.0 ± 2.4	36 ± 5	490 ± 30
S10	0–5	0.28	N.M.	23.2 ± 1.4	146 ± 9	41.8 ± 2.1	26.2 ± 1.7	39 ± 3	620 ± 30
S11	0–5	0.22	N.M.	26.4 ± 2.6	191 ± 17	40 ± 3	20 ± 3	36 ± 6	510 ± 40
S12	0–5	0.17	N.M.	5.0 ± 1.0	88 ± 10	46 ± 3	27.2 ± 2.6	43 ± 5	600 ± 30

f_{org} is the fraction of organic matter in the oven-dry sample, and ρ_b is the dry bulk density.
^{226}Ra is determined through ^{214}Pb. N.M. not measured.
Radionuclide activity concentrations refer to the date of sampling (Table 1).

Table 4
Radionuclide activity concentrations and concentration ratios in roots ($_R$) and aerial parts ($_{AP}$) of plants in Chréa National Pak.

Sample	^{137}Cs	^{210}Pb	^{212}Pb	^{226}Ra	^{228}Ra	^{40}K
	Activity concentrations (Bq kg^{-1})					
$S9_R$	23 ± 3	440 ± 50	10.6 ± 1.7	10 ± 4	12 ± 5	240 ± 40
$S10_R$	7.4 ± 0.8	170 ± 20	17.2 ± 2.5	11.5 ± 2.4	14 ± 3	400 ± 40
$S11_R$	5.3 ± 0.4	105 ± 12	8.1 ± 1.2	3.9 ± 1.0	6.6 ± 1.6	189 ± 18
$S12_R$	1.7 ± 0.3	58 ± 7	6.5 ± 1.0	4.4 ± 1.2	4.5 ± 1.4	189 ± 18
$S9_{AP}$	3.6 ± 0.3	174 ± 19	2.7 ± 0.5	3.7 ± 0.9	2.8 ± 1.0	570 ± 50
$S10_{AP}$	1.8 ± 0.3	105 ± 12	2.8 ± 0.7	1.7 ± 0.8	4.3 ± 1.4	770 ± 70
$S11_{AP}$	2.1 ± 0.4	79 ± 10	3.5 ± 0.8	1.8 ± 1.0	2.9 ± 1.5	650 ± 60
$S12_{AP}$	N.D.	23 ± 4	1.0 ± 0.5	1.2 ± 0.8	N.D.	253 ± 27
	Concentration ratios					
CR $S9_R$	0.22 ± 0.03	1.07 ± 0.15	0.32 ± 0.06	0.46 ± 0.17	0.33 ± 0.15	0.50 ± 0.09
CR $S10_R$	0.32 ± 0.04	1.18 ± 0.15	0.41 ± 0.06	0.44 ± 0.09	0.37 ± 0.09	0.65 ± 0.07
CR $S11_R$	0.20 ± 0.03	0.55 ± 0.08	0.20 ± 0.03	0.20 ± 0.06	0.18 ± 0.05	0.37 ± 0.05
CR $S12_R$	0.34 ± 0.10	0.65 ± 0.11	0.14 ± 0.02	0.16 ± 0.05	0.10 ± 0.04	0.31 ± 0.05
CR $S9_{AP}$	0.16 ± 0.02	0.39 ± 0.06	0.26 ± 0.07	0.37 ± 0.16	0.24 ± 0.14	2.3 ± 0.4
CR $S10_{AP}$	0.24 ± 0.05	0.61 ± 0.10	0.16 ± 0.05	0.14 ± 0.07	0.30 ± 0.12	1.9 ± 0.2
CR $S11_{AP}$	0.40 ± 0.08	0.76 ± 0.13	0.44 ± 0.12	0.45 ± 0.29	0.44 ± 0.25	3.5 ± 0.4
CR $S12_{AP}$	–	0.40 ± 0.09	0.16 ± 0.08	0.26 ± 0.19	–	1.3 ± 0.2
Root crops [a]	0.042 (0.001–0.88)	0.015 ($2.4{\cdot}10^{-4}$- 3.3)		0.07 (0.002–56)	0.07 (0.002–56)	
Grasses [a]	0.063 (0.0048–0.99)	0.31 (0.11–1.0)		0.13 (0.0036–1.6)	0.13 (0.0036–1.6)	1.3 (1.2–1.3)

[a] Reference values for roots in root crops and aerial part of grasses, but for K, which corresponds to leaves in leafy vegetables (IAEA, 2010); mean values and range (in brackets).

for ^{210}Pb.

The ^{137}Cs and $^{210}Pb_{exc}$ inventories take large values, but they seem reliable. Soil S4 is located at the highest elevation (Table 1), where the annual rainfall is about 1400 mm. Legarda et al. (2011) reported ^{137}Cs inventories of 4700 Bq m^{-2} (decay-corrected to 2020) for soils in Spain with annual rainfall of 1470 mm. Similar results were reported by Le Roux et al. (2010), with ~5000 Bq m^{-2} of ^{137}Cs for 1440 mm of annual rainfall for soils in French areas low-impacted by Chernobyl. At the Nakhla catchment (South of Tetouan), on seven uncultivated sites ^{137}Cs inventories ranged from 1671 to 3850 Bq m^{-2}, for an average rainfall of 732 mm (Bouhlassa et al., 2000). In the Aknoul catchment (Eastern Rif), the inventory values ranged between 881 and 5788 Bq m^{-2} of ^{137}Cs for a 471 mm of rainfall (Faleh et al., 2005). For the Nakhla watershed in the Moroccan Rif Mountains, Moustakim et al. (2019) reported reference inventories for ^{137}Cs and $^{210}Pb_{exc}$ of 1520 ± 220 Bq m^{-2} and 3700 ± 1400 Bq m^{-2}, respectively, for a site at 683 m a.s.l. receiving 740 mm of annual rainfall. Also in Morocco, Benmansour et al. (2013) reported reference inventories of 1445 Bq m^{-2} and 3305 Bq m^{-2} for ^{137}Cs and $^{210}Pb_{exc}$, respectively, in agricultural soils in Marchouch, 68 km south from Rabat. In woodland soils, as those in the present study, trees can be effective traps for aerosols, enhancing local deposition of atmospheric fallout radionuclides. Core S8 was sampled in a watershed receiving deposits from upstream runoff, what likely contributed to high inventories of both ^{137}Cs and $^{210}Pb_{exc}$.

Zhang et al. (2021) have presented the largest compilation up to date on ^{210}Pb depositional fluxes. The African continent is one of its noteworthy spatial gaps. They reported fluxes over the world ranging from almost zero up to exceeding 2000 Bq $m^{-2}a^{-1}$, with higher values around the geographical latitudes of 30°- 40° N. Authors also reported a positive and statistically significant correlation with annual rainfall for this range

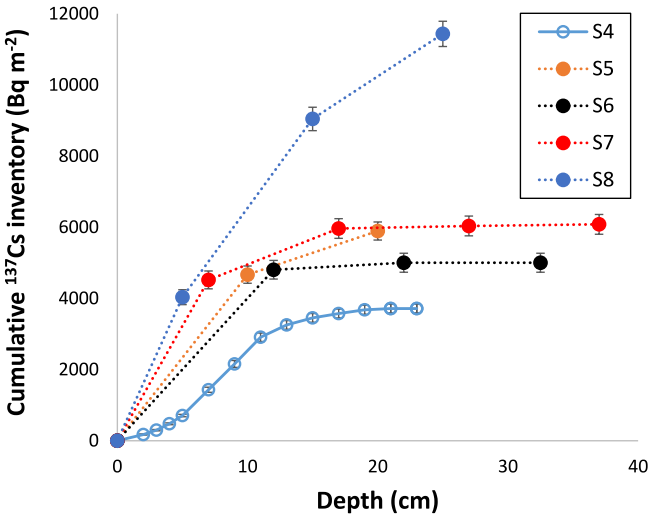

Fig. 3. Cumulative ^{137}Cs inventory as a function of depth for soils S4 to S8 (values correspond to the date of sampling).

Table 5
Total inventories for ^{137}Cs and ^{210}Pb$_{exc}$ and ^{210}Pb$_{exc}$ fluxes in soils from Chréa National Park.

Soil	^{137}Cs inventory (Bq m^{-2})			^{210}Pb$_{exc}$ inventory (Bq m^{-2})			^{210}Pb$_{exc}$ flux (Bq m^{-2}a^{-1})		
S4	3620	±	120	9000	±	900	280	±	27
S5	5890	±	250	12400	±	900	385	±	29
S6	5000	±	270	5400	±	700	169	±	22
S7	6080	±	280	7400	±	1000	230	±	30
S8	11400	±	400	14800	±	1000	460	±	30

Inventories for ^{137}Cs are referred to July 7th, 2020

of latitudes. Other studies have noticed the relevant contribution of Saharan dust events to the annual ^{210}Pb$_{exc}$ flux (e.g., García-Orellana et al., 2006).

After passing Kolmogorov-Smirnov and Shapiro-Wilk normality tests for the variables elevation (Table 1) and total inventories of ^{137}Cs and ^{210}Pb$_{exc}$ (Table 5), only the negative correlation between ^{137}Cs inventories and elevation of the sampling points was statistically significant ($r^2 = 0.89$, $p = 0.016$).

A statistical correlation study has been conducted for the following variables characterizing the surficial soil samples from Chréa National Park (Tables 2 and 3): h (elevation above sea level); OM (organic matter content, determined through LOI %); ρ_b (bulk density); ^{210}Pb$_{exc}$ and ^{137}Cs activity concentrations in the uppermost slice of thickness Δx (cm); and their values ^{210}Pb$_{exc}|_X$ and ^{137}Cs$|_X$, scaled to the 0–5 cm interval by the factor $\Delta x/5$. All the variables passed the Kolmogorov-Smirnov normality test. Table S2 (in ESM) reports the Pearson correlation coefficient matrix.

The OM shows statistically significant positive correlation with h, ^{210}Pb$_{exc}|_X$ and ^{210}Pb$_{exc}$, and negative correlation with ρ_b. The variable ^{137}Cs shows statistically significant positive correlation with ^{210}Pb$_{exc}|_X$ and ^{210}Pb$_{exc}$. Multiple regression models relating ^{137}Cs and ^{210}Pb$_{exc}$ with h, ρ_b and OM were not statistically significant. In summary, the surficial activity concentrations of both fallout radionuclides are statistically correlated, and the concentration of ^{210}Pb$_{exc}$ increases with OM, and this last with h.

Table 4 reports the radionuclide activity concentrations measured in vegetal tissues. In all the cases concentrations in roots were higher than in the aerial parts, by an averaged factor ranging from 2.0 (^{210}Pb) to 4.7 (^{212}Pb). Exception was ^{40}K, whose concentrations in roots were about the half of those found in the aerial parts.

The estimated concentration factors (section 2.6, Table 4) can be compared against the reference values (means and ranges) reported by IAEA (2010). The mean *CR* value found for ^{40}K in the aerial parts of the plants (2.3 ± 0.9, mean and standard deviation) compares well with the IAEA reference (1.3; with only two data reported). No reference values are available for roots. For the other studied radionuclides, present results are overall much higher than the reference mean values, but being within the reported ranges (Table 4).

For ^{226}Ra and ^{228}Ra, the mean *CR* values found in this work for roots (0.31 ± 0.15 and 0.25 ± 0.12, respectively) are about a factor 4 higher than the IAEA reference mean (0.07), while those for aerial parts (0.31 ± 0.15 and 0.32 ± 0.10) are higher by a factor 2–3. These results can be seen as being site and plant specific, with a likely overestimation in the CR for roots due to partial contamination of samples with mineral soil. No reference values are provided for ^{212}Pb, but it closely follows the behaviour of ^{228}Ra, also from the ^{232} Th day series.

For ^{137}Cs, the mean *CR* values for aerial parts and roots found in this work are higher than the IAEA (2010) reference means by a factor 4 and 6, respectively. These factors are higher, but of the order than those found for Ra isotopes. These factors would be even higher for a thicker standardized soil layer, because of the typical decline with depth of ^{137}Cs concentrations in soils.

For ^{210}Pb, the mean *CR* in the aerial parts is only a factor 1.7 higher than the IAEA reference mean value (Table 4), while in roots it is about two orders of magnitude higher, but still within the reported ranges. The standardized soil layer cannot explain this high value. By comparison with other radionuclides, it is unlikely that reason was the contamination of samples by mineral solids. Consequently, these results can be seen as being site and plant specific.

The concentrations of major and some trace elements (Table S1) are of the order of magnitude of their reported abundances in the earth's crust (Haynes et al., 2016), also shown in Table S1. They reflect the particular lithological fingerprint of the study area, rich in Si, and with moderate contents of Fe and Al. It is worth noting that analyses correspond to the bulk soil matrix, so the samples have high content of C, mostly associated to the OM. Data shows different trends of change with depth, which will be discussed further below (section 3.4).

3.2. *Depth profiles of volumetric concentrations of ^{137}Cs and ^{210}Pb$_{exc}$ in core S4, versus CDE analytical solutions*

The ^{137}Cs and ^{210}Pb$_{exc}$ mass activity concentrations in Table 1 can be converted into volumetric concentrations after multiplying by the bulk density and the scaling factor for unit conversion. Then, Eq. (1) can be applied for ^{137}Cs after fitting the values for parameters D and v. Similarly, Eq. (2) applies for ^{210}Pb.

The analytical solution of the simplified CDE (Eq. (1)) labelled as "Analytical-1" in Fig. 4 assumes that the total ^{137}Cs inventory resulted from a single pulse at 1963, coinciding with the maximum atmospheric fallout. Thus, the solution is evaluated for the elapsed time $t = 54$ years. A reasonable fit (Fig. 4) is achieved with an effective diffusion coefficient of 0.14 cm^{2}a^{-1} and the effective convective velocity of 0.132 cm a^{-1}. According to the soil classifications by IAEA (2010), the reference values for D and v are, respectively, of 0.22 cm^{2}a^{-1} and 0.09 cm a^{-1} (^{137}Cs from weapons fallout, all soils). Furthermore, when estimating the retardation factor with a reference value of $k_d \sim 10^3$, it results a convection velocity $v' \sim 1320$ mm a^{-1}, which is close to the annual rainfall rate. According to this model (Eq. (1)), after another elapsed time of 50 years (i.e., at date 2067), the maximum volumetric concentration would be around 0.010 Bq cm^{-3} and located at 15 cm depth.

The approach of Eq. (2) provides a very poor description of the experimental data for ^{210}Pb$_{exc}$, as shown in Fig. 4. At least the order of magnitude is reproduced when using the same parameters values for D and v than for ^{137}Cs.

A different approach is possible for both radionuclides, also based in the simplified CDE but accounting for a fast initial distribution (labelled

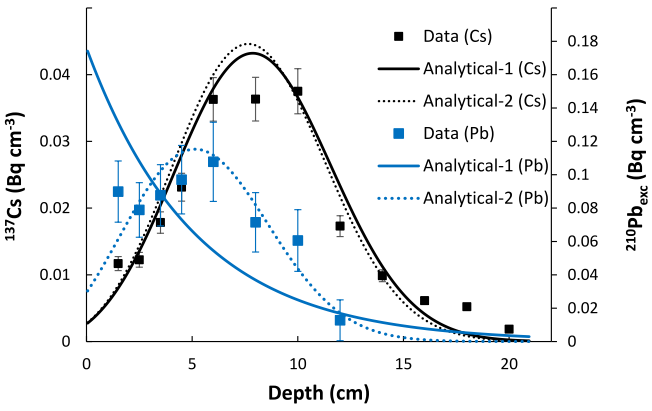

Fig. 4. ^{137}Cs and ^{210}Pb$_{exc}$ (Bq cm^{-3}) versus depth in soil S4: experimental data (vertical bars are 1σ analytical uncertainties), and analytical solution by Eq. (1) (for ^{137}Cs after an elapsed time of 54 y, and parameter values $D = 0.14$ cm^{2}a^{-1} and $v = 0.132$ cm a^{-1}) and Eq. (2) (for ^{210}Pb$_{exc}$ with parameter values $D = 0.14$ cm^{2}a^{-1}, $v = 0.132$ cm a^{-1} and $F = 280$ Bq m^{-2}a^{-1}), both denoted as "Analytical-1". "Analytical-2" applies Eq. (1) with t = 0.003 y for ^{137}Cs ($D = 2400$ cm^{2}a^{-1}, $v = 2300$ cm a^{-1}) and ^{210}Pb$_{exc}$ ($D = 2260$ cm^{2}a^{-1}, $v = 1450$ cm a^{-1}).

as Analytical-2 in Fig. 4). One can consider a pulsed input at the beginning of a rain event during which the infiltration velocity remains constant for hours or few days. The assumption of instantaneous and reversible uptake holds during the infiltration event, after what the activity profile would become irreversibly fixed. The empirical profile after large elapsed times would be the superposition of a series of these "initial-distribution" patterns (after radioactive-decay correction), further perturbed by tiny effective diffusion and convection. At this stage, we can use Eq. (1) for characterizing a fast initial distribution and neglect further post-depositional processes. Thus, and just as concept-demonstration, Analytical-2 uses Eq. (1) for both ^{137}Cs and ^{210}Pb$_{exc}$, evaluated for t = 0.003 y (~1 day). The value of J_o is the empirical inventory, and the values for D and v are consistently fitted.

Now the true percolation velocities are of the order of few cm h^{-1} (Hillel, 1971), so the effective convection velocities are expected to be about four orders of magnitude higher than those found with the Analytical-1 approach. Fig. 4 shows the computed profiles (by Eq. (1)) for ^{137}Cs and ^{210}Pb$_{exc}$. The effective diffusion coefficient was 2400 cm^{2}a^{-1} for ^{137}Cs and 2260 cm^{2}a^{-1} for ^{210}Pb$_{exc}$, while the effective convection velocities were 2300 cm a^{-1} and 1450 cm a^{-1} (or 0.26 cm h^{-1} and 0.16 cm h^{-1}), respectively. In both cases, the pulsed input fitted the empirical inventories, which can be seen as the linear superposition of several identical events without post-redistribution processes. Differences in velocities are explained by a k_d value for ^{210}Pb about twice that for ^{137}Cs. According to this interpretation, after an elapsed time of 50 years, the position of the ^{137}Cs would be at the same depth (7.75 cm) and its size would decrease only by radioactive decay to 0.015 Bq cm^{-3}.

The above numerical exercises show that, despite the quality of the fits to analytical functions, the interpretation of ^{137}Cs and ^{210}Pb$_{exc}$ depth profiles in soils is not straightforward, even using the same simplified CDE. The so derived parameters, v and D, do not necessarily reflect the physical reality and they lack of predictive value. Moreover, Eq. (1) implicitly assumes uniform bulk density and porosity, what is not the case for S4 (see Table 2). Thus, using a uniform mean value for bulk density would drastically change the shape of the ^{137}Cs profile, now showing a pronounced plateau in the 0–8 cm interval. This would lead to different fitted values for v and D, and then to different predictions. This highlights the need of a more comprehensive understanding of the basic processes governing the depth-distribution in soils of fallout radionuclides. A relevant task for this goal is improving our understanding on how rhizospheres can affect the dynamics of the pore fluid and the partitioning of radionuclides in a multiphasic soil matrix.

3.3. *Polyphasic structure of the soil core S4*

The approach of section 2.5 has been applied with the empirical measurements of f_w and f_{org} (Table 2). At large depths the fraction of organic matter takes the basal value $f_{org,D} = 0.05$, which has been assumed to be uniform in the entire core. Due to its small value when compared against the OM-rich upper soil, this simplification seems reasonable. We adopted the value $f_T = 0.3$ for plant roots, and the representative densities of the different soil components, as summarized in section 2.5. Results are shown in Fig. 5.

Plant roots occupy about 45% of the soil volume in the 0–10 cm region, and then this percentage sharply decreases with depth. The volume occupied by the mineral fraction is less than 5% at the soil surface and asymptotically increases with depth up to values around 65%. Plant roots do not only displace the mineral soil, but also locally enhance the global porosity. As described in the methodology, the soil site was waterlogged for facilitating the coring operation, and then stored in vertical position. At the time of slicing, the upper soil had lost part of its gravity water, so that the fraction of volume occupied by air was quite noticeable, as seen in Fig. 5. The summation of the above last two fractions compose the total porosity, which is about 75% at the soil surface, and sharply decreases up to almost constant values around 30%.

Several insights can be obtained from Fig. 5: i) The assumption of uniform bulk density and porosity, as done in Eqs. (1) and (2), is not a reliable description of the physical environment of the soil. ii) Roots occupy an important fraction of the soil volume, which cannot be accounted as porosity, and through which the convective-diffusive transport does not operate. iii) The uncompensated electrical charges at the external surfaces of the mineral solids (Hillel, 1971) makes the mineral fraction acting as a filter for the dynamical uptake of dissolved radionuclides in the pore fluid. The low mineral bulk density in the upper soil facilitates the depth penetration of fallout radionuclides during infiltration events. iv) Radionuclide uptake by plants may involve different processes (e.g., roots excrete organic acids to create micro-environments with availability of nutrients and dissolved elements) and different kinetics and time-scales (e.g. continuous or episodic).

It has been often argued in the scientific literature that ^{210}Pb$_{exc}$ strongly correlates with OM (e.g., Itthipoonthanakorn et al., 2019). This correlation is also found in the soil core S4, as shown in Fig. 6 ($r^2 = 0.90$; $p = 0.0003$).

The reason for the above correlation may not be a preferential fixation of ^{210}Pb to OM (see discussion further below) but just the spatial co-occurrence of two independent trends of decrease with depth: i) the density of roots decreases with depth, ii) ^{210}Pb$_{exc}$ concentrations decrease with depth because its cumulative retention in the mineral fraction during infiltration events (Fig. 4).

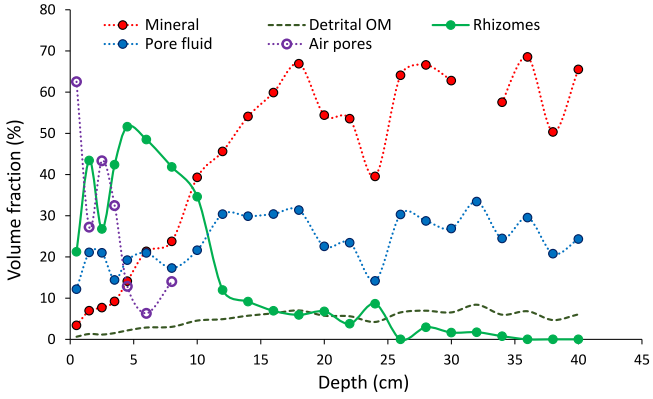

Fig. 5. Estimates of the volume fractions of the different components of the polyphasic soil for core S4, following the conceptual model and the methodology of section 2.5 with the physical measurements reported in Table 2.

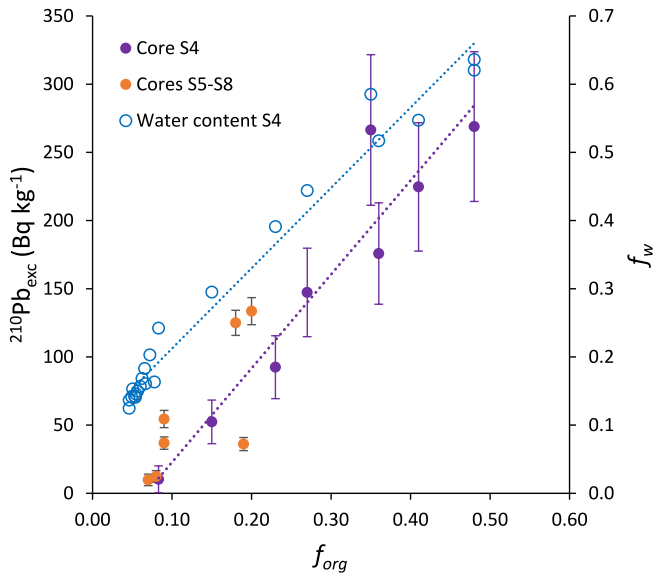

Fig. 6. Correlation between the fraction of OM f_{org}, and the $^{210}Pb_{exc}$ activity concentrations in the different slices of the soil core S4 (also reported values for the low-resolution cores S5 to S8). The water content also correlates with f_{org}, what its explained by the tissue water and the enhanced porosity around plant roots.

The water content in core S4 reflects the transient stage at the time of slicing. It also correlates with f_{org} ($r^2 = 0.98$; $p = 0.0000$; Fig. 6), what is explained by both the tissue water and the enhanced porosity around plant roots.

3.4. Concentration factors and the dilution effect of OM

Fig. 7 shows the depth profiles of concentrations of natural radionuclides in soil core S4, after normalization to their arithmetic means in the 0–40 cm interval (raw data in Table 2). These concentrations refer to the bulk sediment matrix. They show a common pattern of asymptotic increase with depth. Changes in the isotopic composition of the surficial soils are not expected from pedology, so here we explore potential effects of OM.

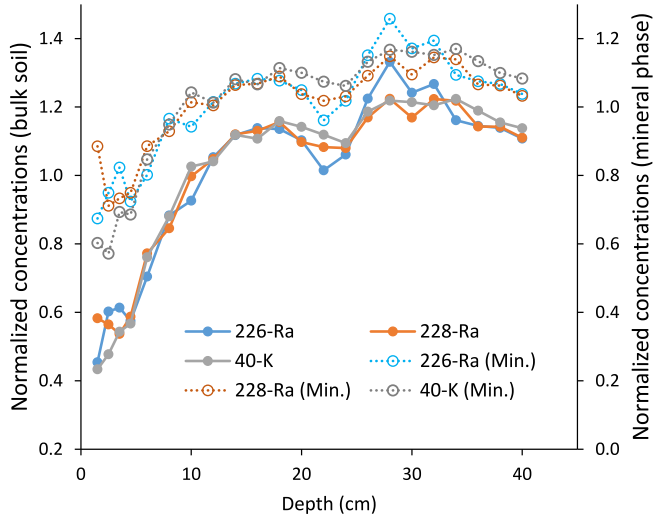

Fig. 7. Depth profiles of concentrations of natural radionuclides in the soil core S4, after normalization to their arithmetic means in the 0–40 cm interval (raw data in Table 2; they correspond to the bulk sediment matrix; error bars not depicted for the sake of clarity). Also plotted are the normalized profiles for their concentrations in the mineral phase, as estimated after Eq. (3) with $CR = 0.31$ for ^{226}Ra, $CR = 0.25$ for ^{228}Ra, and $CR = 0.46$ for ^{40}K (mean values reported in Table 4). Note that the left vertical axis has been uniformly displaced (without rescaling) for the sake of clarity. By definition, normalized concentrations are dimensionless ($x_{i,\,norm} = x_i/\bar{x}$).

After Iurian et al. (2021), in OM-rich soils (and vegetated sediments), the radionuclide activity concentrations in the mineral phase A_{min}, can be estimated from their measured values in the bulk soil matrix, A_b, and the site and plant specific concentration ratios (CR). When neglected corrections for saline pore fluids, the following equation locally applies for each soil slice (Iurian et al., 2021):

$$A_{min} \cong \frac{A_b\left(1 - CR\, f_{org}\right)}{1 - f_{org}} \tag{3}$$

A_{min} has been estimated for the three natural radionuclides in Fig. 7 by using CR values from Table 4. The corresponding normalized values (to their arithmetic means in the core) are shown in Fig. 7. They are more uniform with depth below the rhizosphere (see Fig. 5), but they show a depletion in the 0–10 cm interval, which could be at least partially explained by the role of rhizospheres. The acid micro-environments they create promote leaching and percolation, and the extraction and export to aerial parts of trace elements from the mineral soil. It is worth noting that the application of Eq. (3) in a local basis is justified when the product $CR\, f_{org} \ll 1$, and then the major effect is a matrix dilution effect through the factor $(1 - f_{org})$, as discussed in Iurian et al. (2021).

Further insights on the effect of rhizospheres in the depth distribution of concentrations of major and trace elements in the bulk soil matrix can be obtained from data reported in Table S1 (in ESM). Fig. 8 plots such depth profiles of concentrations for a set of elements, after being normalized to their arithmetic means for facilitating comparison.

Fig. 8 reflects the effect of a composite soil matrix consisting in organic and mineral fractions whose relative proportions vary with depth. Thus, the concentrations of Si, Fe, Al and Rb are lower within the rhizosphere, as above observed for the natural radionuclides. This pattern would be explained by both, element-CR values lower than unity, and the above commented leaching-percolation effect. Other elements, such as C, P and Sr are more abundant in the vegetal tissues, so their concentrations follow the same pattern of decrease with depth than plant roots. Carbon (C) is the major constituent of vegetal tissues, and it is fixed from the atmosphere by photo-assimilation. Phosphorus is a macro-nutrient, and Sr mimics Ca. Their distribution likely obey to their selective adsorption by plants from the acid micro-environments of

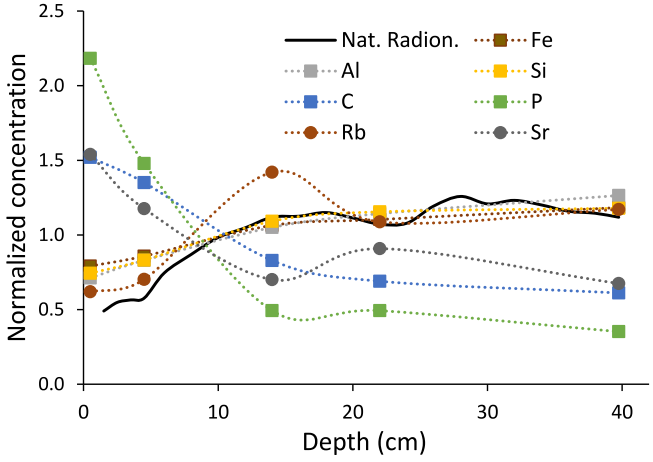

Fig. 8. Depth profiles of normalized (to their arithmetic mean values) concentrations of major and trace elements (Table S1, ESM) in the bulk sediment matrix of soil core S4. The distribution of natural radionuclides (from Fig. 7) is depicted for the sake of comparison. By definition, normalized concentrations are dimensionless.

rhizospheres, and their recycling over the time scales of pedology.

A similar effect is expected to occur for the fallout radionuclides ^{137}Cs and ^{210}Pb$_{exc}$. Fig. 9 shows their respective depth profiles of concentrations in both, the dry bulk matrix and the mineral phase. Differences are apparent for ^{137}Cs in the 0–10 cm interval where the OM is higher due to plant roots (see Fig. 5). For ^{210}Pb, the site specific *CR* value for plant roots is close to unity (Table 4), so concentrations in the bulk matrix and in the mineral phase are virtually coincident (Fig. 9). It is worth noting how the ^{210}Pb$_{exc}$ profile takes negative values below 14 cm depth, which is consistent with ^{222}Rn exhalation (from in situ decay of ^{226}Ra) under non-saturated conditions.

From Eq. (3), it can be inferred that the fraction of the radionuclide activity in the bulk matrix which is attached to the mineral phase is $1 - CRf_{org}$. Thus, for ^{137}Cs, with $CR = 0.27$ for plant roots, the fraction attached to the mineral phase ranges from 1 for $f_{org} = 0$, to 0.88 for $f_{org} = 0.50$. With the same limits for f_{org}, the fraction in the mineral phase for ^{210}Pb ranges from 1 to 0.99 and from 1 to 0.55 when using the IAEA reference mean value or the site and plant specific one reported in this work (Table 4), respectively.

The profiles of activity concentrations for the mineral phase are more informative on the physical-chemical process involved in the dynamical and fast uptake by mineral solids of dissolved radionuclides moving through the pore fluid during infiltration events. Thus, the high particle-reactive ^{210}Pb shows an exponential pattern of penetration, while the more mobile ^{137}Cs shows a plateau in the upper soil and longer penetration tails (see IAEA, 2010 for reference k_d values).

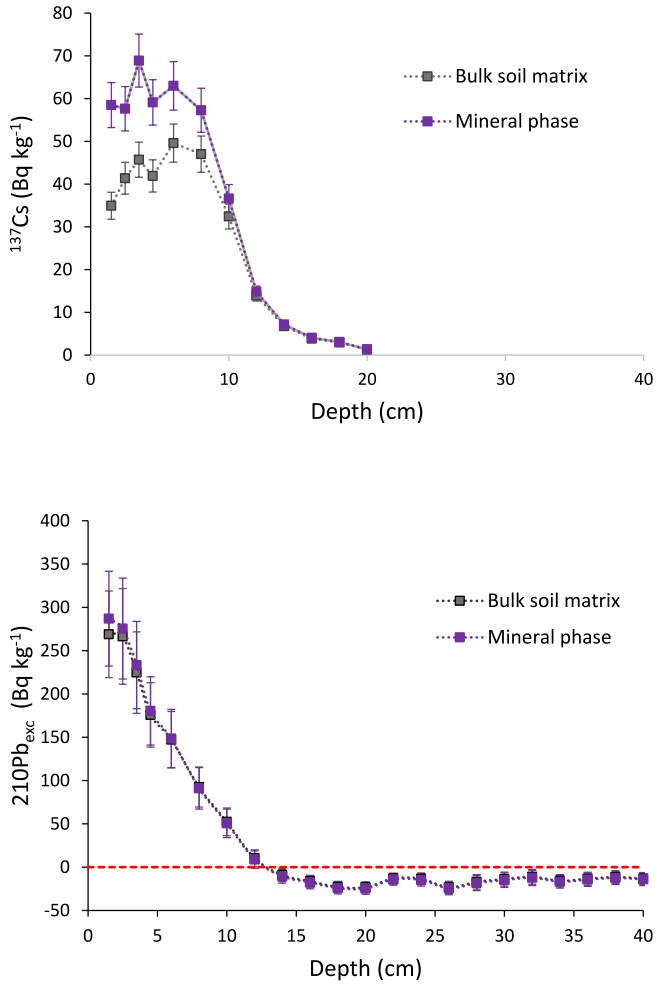

Fig. 9. Depth profiles of ^{137}Cs (first panel) and ^{210}Pb$_{exc}$ (second panel) concentrations in both the dry bulk matrix and the mineral phase of soil core S4. The latter have been estimated after Eq. (3) with $CR = 0.27$ for ^{137}Cs, $CR = 0.31$ for ^{226}Ra, and $CR = 0.9$ for ^{210}Pb (see mean values in Table 4).

3.5. *Modelling ^{137}Cs profiles in the mineral phase of soils using CDE with fast initial distributions*

This section presents an exploratory modelling study based upon the following set of assumptions: i) During episodic infiltration events in soils, radionuclides distribute in depth as result of the convective-diffusive transport through the pore fluid and the kinetic uptake by the mineral phase. ii) Post-depositional processes, including further leaching and percolation, can be overall described as an effective convective-diffusive process in the space of the mineral phase. iii) The relevant depth scale is the mineral mass-depth, $m_{min}(x) = \int_0^x (1 - f_{org})\rho_b(x')dx'$, the continuity equation holds for A_{min}, the process i) is described by a depth-distributed source term, $s(m_{min}, t)$, and process ii) by an effective accretion, w_{min} (mineral g cm^{-2}a^{-1}), and an effective diffusion coefficient, D_{min}. iv) For simplicity, it will be assumed that all the percolation events results in the same $s(m_{min})$, so that historical series of deposition rates, $F(t)$, can be used for modelling the ^{137}Cs fallout history, while steady-state solutions under a constant fallout rate can be a reasonable proxy for ^{210}Pb$_{exc}$.

For simplicity in notation, the sub-index "min" will be omitted in what follows. The mineral bulk density, $\rho_{b,\,min}$ varies with depth (and this is accounted by using the m_{min} scale), but it is assumed to be steady state. Then, adapting from Abril and Gharbi (2012), the continuity equation for the radionuclide concentration in the mineral phase is:

$$\frac{\partial A}{\partial t} = -\lambda A - w\frac{\partial A}{\partial m} + \frac{\partial}{\partial m}\left(D\frac{\partial A}{\partial m}\right) + s(m) - u(m)A \quad (4)$$

$$F(t) = \int_0^\infty s(m,t)dm \quad (5)$$

In Eq. (4) λ is the radioactive decay constant of the studied radionuclide, and $u(m)$ is the rate at which the radionuclide is retired from the mineral phase by plant uptake. As above discussed, at a first approach and with present data, $u(m)$ can be neglected for ^{137}Cs. Owing to the high k_d value of Cs, the porewater phase does not need to be explicitly considered, since after each fast distribution process (here described through $s(m,t)$), virtually all the activity is bound to the mineral phase.

For $s(m,t)$ the following common parameterization has been adopted:

$$s(m,t) = \frac{K_n(t)}{1 + e^{\alpha(m-m_a)}} \quad (6)$$

This parameterization allows for an almost constant value in the upper soil that then declines to zero around the mineral mass depth m_a with an exponential scaling factor, α. $K_n(t)$ is the normalizing constant needed to fulfil Eq. (5). The depth-dependent effective diffusion coefficient has been parameterized with a similar function:

$$D(m) = \frac{D_o}{1 + e^{\alpha'(m-m_a')}} \quad (7)$$

In the case of ^{137}Cs, for $F(t)$ the common use considers the available historical records at reference sites in the North Hemisphere, modified by a site-specific scaling factor. In this work, we used the atmospheric deposition record in U.K., as adapted by Iurian et al. (2021) using data from Wright (2016). The site-specific adaptation consisted in a scaling factor, selected in such a way that the integrated atmospheric deposition matched the measured total inventory.

Fig. 10 shows the numerical solution of Eq. (4) with the above adapted $F(t)$, with $s(m,t)$ given by Eq. (6) with $m_a = 4.2$ g cm^{-2} and $\alpha = 0.9$ g^{-1}cm^2, $w = 0$, and $D(m)$ given by Eq. (7) with $m_a' = m_a$, $\alpha' = \alpha$, and $D_o = 0.1$ g^{2}cm^{-4}a^{-1}. This produces a reasonable description of the

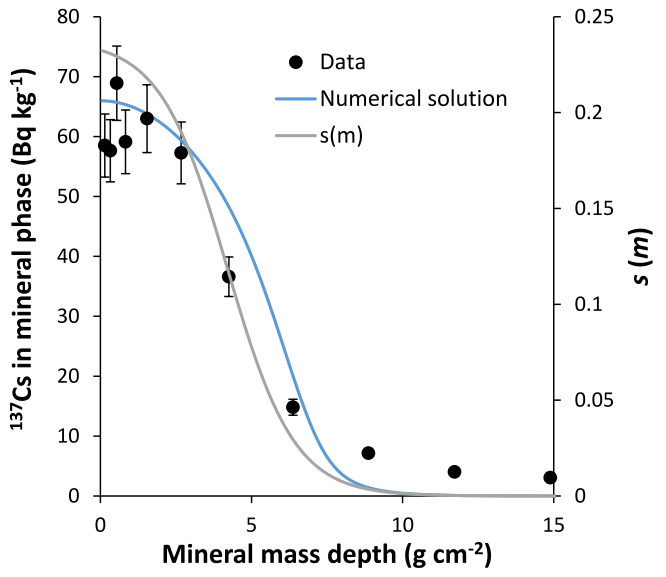

Fig. 10. ^{137}Cs activity concentrations in the mineral phase in soil S4 versus mineral mass depth. Data have been estimated by Eq. (3) from raw data in Table 2; $s(m)$ is the initial fast distribution (Eq. (6)) normalized to unit flux (Eq. (5)). The continuous blue line is the numerical solution of Eq. (4) with the above $s(m)$, the depositional history $F(t)$ adapted from Iurian et al. (2021), $w = 0$ and D given by Eq. (7). (For interpretation of the references to colour in this figure legend, the reader is referred to the Web version of this article.)

empirical data set.

The numerical solution shown in Fig. 10 has the value of concept-demonstration, and it does not provide the best possible fit to data. Indeed, it is expected that a wide set of combinations of $s(m,t)$ and $D(m)$ functions can reasonably fit the empirical data, and they can be fine-tuned to better reproduce the long penetration tail. Fig. 10 highlights that the study of the distribution and migration of fallout radionuclides in soils is still an open question, and that the widely accepted method based upon analytical solutions of a simplified CDE may not be a reliable representation of the real world, and thus it lacks of predictive value.

With the site and plant specific *CR* value for ^{210}Pb, applying Eq. (4) would require an explicit parametrization of $u(m)$, what is beyond the scope of the present work. Future research works should consider the numerical simulation of the convective-diffusive process and the uptake kinetics to find out initial fast distributions $s(m)$ from basic principles instead of postulating them ad hoc.

4. Conclusions

Inventories of fallout radionuclides ^{137}Cs (artificial) and ^{210}Pb$_{exc}$ (natural) in soils of the Chréa National Park are typical from global fallout in high precipitation areas in the Northern Hemisphere, being, respectively, of 3620 ± 120 Bq m^{-2} and 9000 ± 900 Bq m^{-2} at site S4 (high resolution soil core).

The activity concentrations of ^{137}Cs and ^{210}Pb$_{exc}$ in surficial soil samples were statistically correlated at 95% confidence level. Concentrations of ^{210}Pb$_{exc}$ increased with OM, and this last correlated with the elevation above sea level of the sampling site.

The dominant plant species in the vegetal cover of soils were *Poa pratensis* L. and *A. mauritanicus* – A. The empirically determined concentration ratios (*CR*) in roots and aerial parts for the studied radionuclides were higher than the literature reference mean values, but being within the reported ranges. They were around 0.3 for ^{137}Cs and Ra isotopes. For ^{40}K, the *CR* was around 2.3 and 0.46 in the aerial parts and roots, respectively. For ^{210}Pb, a high value was found for roots, with *CR* around 0.9.

Depth distributions of volumetric concentrations of ^{137}Cs and ^{210}Pb$_{esx}$ were fitted to the analytical solutions of a simplified CDE reported in literature. For ^{137}Cs, the fit (at a time of observation of 54 years after the maximum bomb fallout) was reasonably good, with fitting parameters well in the range of reference values. For ^{210}Pb$_{exc}$, the exponential pattern of the steady state solution gave a poor description of data.

The above profiles can be alternatively explained as the composite result of fast depth-distributions following infiltration events. The analytical solution of the CDE for a time of observation of 1 day, with a convective term describing realistic infiltration velocities, provided a good description of both, ^{137}Cs and ^{210}Pb$_{esx}$ profiles. This limits the common accepted interpretation of data and its predictive use.

This work presented a simple conceptual model of a polyphasic soil, including rhizospheres. Its application to soil core S4 provided a realistic description of the physical environment, where roots occupied about 45% of the soil volume in the 0–10 cm interval (Fig. 5). High porosity was found around roots, while the inorganic phase was low in this region.

The composite soil matrix, consisting in organic and mineral fractions whose relative proportions vary with depth, can explain the observed depth-distributions of ^{40}K, Ra isotopes, and the studied major and trace elements (Figs. 7 and 8). Those elements linked to the mineral phase show low concentrations within the rhizosphere, while Carbon and the macro and micronutrients show their highest concentrations within this zone.

The profiles of concentration in the mineral phase are more informative for understanding the dynamical and fast uptake by mineral solids of dissolved radionuclides moving through the pore fluid during infiltration events. This has been illustrated with the numerical modelling of the ^{137}Cs profile in the mineral phase of the soil core S4 by using a CDE with fast initial distributions (Fig. 10).

Declaration of competing interest

The authors declare that they have no known competing financial interests or personal relationships that could have appeared to influence the work reported in this paper.

Acknowledgements

This work was supported by the Centre de Recherche Nucléaire d'Alger (CRNA).

The authors would like to really thank Mrs. F. Takarli and Mr. M. Ziar from Chréa National Park for the help providing during sampling. Thanks are given to Mrs A. Hammadi and M. A. Arabi from the CRNA by their assistance providing the IAEA reference materials and the WDXRF analysis, respectively. Thanks are given also to students for providing help during sampling and treatment: H. Laouar, H. Lallali, S. Boudouaou, H. Attia, T. Rabia, O. Mecibah, M. Nekkaa and R. Zorgani.

References

Abril, J.M., Gharbi, F., 2012. Radiometric dating of recent sediments: beyond the boundary conditions. J. Paleolimnol. 48, 449–460. https://doi.org/10.1007/s10933-012-9622-5.

Azbouche, A., Belamri, M., Morsli, B., Hamoudi, A., Melzi, Z., 2017. Study of ^{137}Cs redistribution in semi-arid land of western Algeria for soil loss assessment. J. Agric. Environ. Int. Dev. 111 (1), 141–155.

Baggoura, B., Noureddine, A., Benkrid, M., 1998. Level of natural and artificial radioactivity in Algeria. Appl. Radiat. Isot. 49 (7), 867–873. https://doi.org/10.1016/S0969-8043(97)10005-7.

Barros, H., Abril, J.M., 2005. Constraints in the construction and/or selection of kinetic box models for the uptake of radionuclides and heavy metals by suspended

particulate matter. Ecol. Model. 185, 371–385. https://doi.org/10.1016/j.ecolmodel.2005.01.002.
Barros, H., Abril, J.M., 2008. Kinetic box models for the uptake of radionuclides and heavy metals by suspended particulate matter: equivalence between models and its implications. J. Environ. Radioact. 99, 146–158. https://doi.org/10.1016/j.jenvrad.2007.07.007.
Benmansour, M., Mabit, L., Nouira, A., Moussadek, R., Bouksirate, H., Duchemin, M., Benkdad, A., 2013. Assessment of soil erosion and deposition rates in a Moroccan agricultural field using fallout ^{137}Cs and ^{210}Pb$_{ex}$. J. Environ. Radioact. 115, 97–106. https://doi.org/10.1016/j.jenvrad.2012.07.013.
Bossew, P., Kirchner, G., 2004. Modelling the vertical distribution of radionuclides in soil. Part 1: the convection–dispersion equation revisited. J. Environ. Radioact. 73, 127–150. https://doi.org/10.1016/j.jenvrad.2003.08.006.
Bouhlassa, S., Moukchane, M., Aiachi, A., 2000. Estimates of soil erosion and deposition of cultivated soil of Nakhla watershed, Morocco, using ^{137}Cs technique and calibration models. Acta Geol. Hisp. 35 (3–4), 239–249.
Chaif, H., Coppin, F., Bahi, A., Garcia-Sanchez, L., 2021. Influence of non-equilibrium sorption on the vertical migration of 137Cs in forest mineral soils of Fukushima Prefecture. J. Environ. Radioact. 232, 106567. https://doi.org/10.1016/j.jenvrad.2021.106567.
Ehlken, S., Kirchner, G., 2002. Environmental processes affecting plant root uptake of radioactive trace elements and variability of transfer factor data: a review. J. Environ. Radioact. 58, 97–112. https://doi.org/10.1016/S0265-931X(01)00060-1.
Faleh, A., Bouhlassa, S., Sadiki, A., Navas, A., Aboutaher, A., 2005. Assessment of soil erosion by fallout ^{137}Cs in the Abdelali basin (Rif of N Morocco). Cuaternario Geomorfol. 19 (1–2), 15–22.
García-Orellana, J., Sánchez-Cabeza, J.A., Masqué, P., Ávila, A., Costa, E., Loÿe-Pilot, M. D., Bruach-Menchén, J.M., 2006. Atmospheric fluxes of ^{210}Pb to the western Mediterranean Sea and the Saharan dust influence. J. Geophys. Res. 111, D15305. https://doi.org/10.1029/2005JD006660.
Haynes, William M., Lide, David R., Thomas, J., Bruno, 2016. CRC Handbook of Chemistry and Physics: A Ready-Reference Book of Chemical and Physical Data. CRC Press, Boca Raton, Florida.
He, Q., Walling, D.E., 1997. The distribution of fallout ^{137}Cs and ^{210}Pb in undisturbed and cultivated soils. Appl. Radiat. lsot. 48 (5), 677–690. https://doi.org/10.1016/S0969-8043(96)00302-8.
Hillel, D., 1971. Soil and Water. Physical Principles and Processes. Academic Press, Inc., Orlando, Florida.
IAEA, 2004. Sediment distribution coefficients and concentration factors for biota in the marine environment. In: IAEA Technical Reports Series No. 422, Vienna report, ISSN 0074–1914.
IAEA, 2010. Handbook of parameter values for the prediction of radionuclide transfer in terrestrial and freshwater environments. In: IAEA Technical Reports Series No. 472, Vienna report, ISSN 0074–1914.
Itthipoonthanakorn, T., Dann, S.E., Crout, N.M.J., Shaw, G., 2019. Nuclear weapons fallout ^{137}Cs in temperate and tropical pine forest soils, 50 years post-deposition. Sci. Total Environ. 660, 807–816. https://doi.org/10.1016/j.scitotenv.2019.01.073.
Iurian, A.R., Millward, G.E., Blake, W., Abril Hernández, J.M., 2021. Fine-tuning of ^{210}Pb-based methods for dating vegetated saltmarsh sediments. Quat. Geochronol. 62, 101153. https://doi.org/10.1016/j.quageo.2021.101153.
Kirchner, G., 1998. Applicability of compartmental models for simulating the transport in soils. J. Environ. Radioact. 38, 339–352. https://doi.org/10.1016/S0265-931X(97)00035-0.
Kirchner, G., Strebl, F., Bossew, P., Ehlken, S., Gerzabek, M.H., 2009. Vertical migration of radionuclides in undisturbed grassland soils. J. Environ. Radioact. 100, 716–720. https://doi.org/10.1016/j.jenvrad.2008.10.010.
Knatko, V.A., Skomorokhov, A.G., Asimova, V.D., Strakh, L.I., Bogdanov, A.P., Mironov, V.P., 1996. Characteristics of ^{90}Sr, ^{137}Cs and $^{239,\ 240}$Pu migration in undisturbed soils of southern Belarus after the Chernobyl accident. J. Ennviron. Radioact. 30 (2), 185–196. https://doi.org/10.1016/0265-931X(95)00011-X.
Kurikami, H., Malins, A., Takeishi, M., Saito, K., Iijima, K., 2017. Coupling the advection-dispersion equation with fully kinetic reversible/irreversible sorption terms to model radiocesium soil profiles in Fukushima Prefecture. J. Environ. Radioact. 171, 99–109. https://doi.org/10.1016/j.jenvrad.2017.01.026.
Legarda, F., Romero, L.M., Herranz, M., Barrera, M., Idoeta, R., Valiño, F., Olondo, C., Caro, A., 2011. Inventory and vertical migration of ^{137}Cs in Spanish mainland soils. J. Environ. Radioact. 102, 589–597. https://doi.org/10.1016/j.jenvrad.2011.03.007.
Le Roux, G., Duffa, C., Vray, F., Renaud, P., 2010. Deposition of artificial radionuclides from atmospheric Nuclear Weapon Tests estimated by soil inventories in French areas low-impacted by Chernobyl. J. Environ. Radioact. 101, 211–218. https://doi.org/10.1016/j.jenvrad.2009.10.010.
Liu, W., Li, Y., Yu, H., Saggar, S., Gong, D., Zang, Q., 2021. Distribution of ^{137}Cs and ^{60}Co in plough layer of farmland: evidenced from a lysimeter experiment using undisturbed soil columns. Pedosphere 31 (1), 180–190. https://doi.org/10.1016/S1002-0160(19)60837-4.
Luczak, C., Janquin, M.A., Kupka, A., 1997. Simple standard procedure for the routine determination of organic matter in marine sediment. Hydrobiologia 345, 87–94.
Mabit, L., Benmansour, M., Abril, J.M., Walling, D.E., Meusburger, K., Iurian, A.R., Bernard, C., Tarjan, S., Owens, P.N., Blake, W.H., Alewell, C., 2014. Fallout ^{210}Pb as a soil and sediment tracer in catchment sediment budget investigations: a review. Earth Sci. Rev. 138, 335–351. https://doi.org/10.1016/j.earscirev.2014.06.007.
Matsuda, N., Mikami, S., Shimoura, S., Takahashi, J., Nakano, M., Shimada, K., Uno, K., Hagiwara, S., Saito, K., 2015. Depth profiles of radioactive cesium in soil using a scraper plate over a wide area surrounding the Fukushima Dai-ichi Nuclear Power Plant. Japan. J. Environ. Radioact. 139, 427–434. https://doi.org/10.1016/j.jenvrad.2014.10.001.
Mehra, R., Singh, M., 2011. Measurement of radioactivity of ^{238}U, ^{226}Ra, ^{232}Th and ^{40}K in soil of different geological origins in northern India. J. Environ. Protect. 2, 960–966. https://doi.org/10.4236/jep.2011.27110.
Mishra, S., Sahoo, S.K., Bossew, P., Sorimachi, A., Tokonami, S., 2016. Vertical migration of radio-caesium derived from the Fukushima Dai-ichi Nuclear Power Plant accident in undisturbed soils of grass land and forest. J. Geochem. Explor. 169, 163–186. https://doi.org/10.1016/j.gexplo.2016.07.023.
Moustakim, M., Benmansour, M., Zouagui, A., Nouira, A., Benkdad, A., Damnati, B., 2019. Use of caesium-137 re-sampling and excess lead-210 techniques to assess changes in soil redistribution rates within an agricultural field in Nakhla watershed. J. Afr. Earth Sci. 156, 158–167. https://doi.org/10.1016/j.jafrearsci.2019.04.017.
Nadri, M., Tanha, M.R., Hoeschen, C., Khiari, C., Ioannidou, A., 2019a. Activity concentration and annual effective dose estimation of ^{210}Pb,^{40}K and ^{137}Cs in soils of southern Algeria. Int. J. Environ. Sci. Technol. 16, 6527–6534. https://doi.org/10.1007/s13762-019-02247-0.
Nadri, M., Khairi, C., Ioannidou, A., 2019b. Soil depth profile of ^{137}Cs, ^{210}Pb and ^{40}K in Algeria. Radiat. Eff. Defect Solid 174, 339–348. https://doi.org/10.1080/10420150.2019.1570515.
Ni, Y., Wang, Z., Guo, Q., Zheng, J., Li, S., Lin, J., Tan, Z., Huang, W., 2018. Distinctive distributions and migrations of $^{239+240}$Pu and ^{241}Am in Chinese forest, grassland and desert soils. Chemosphere 212, 1002–1009. https://doi.org/10.1016/j.chemosphere.2018.09.021.
Paul, D., White, W.M., Turcotte, D.L., 2003. Constraints on the ^{232}Th/^{238}Uratio (κ) of the continental crust. Geochem. Geophys. 4 (12), 1102. https://doi.org/10.1029/2002GC000497.
Schimmack, W., Bunzl, K., Zelless, L., 1989. Initial rates of migration of radionuclides from the Chernobyl fallout in undisturbed soils. Geoderma 44, 211–218. https://doi.org/10.1016/0016-7061(89)90030-X.
Schimmack, W., Schultz, W., 2006. Migration of fallout radiocaesium in a grassland soil from 1986 to 2001. Part I: activity–depth profiles of ^{134}Cs and ^{137}Cs. Sci. Total Environ. 368, 853–862. https://doi.org/10.1016/j.scitotenv.2006.03.028.
Smith, J.T., Appleby, P.G., Hilton, J., Richardson, N., 1997. Inventories and fluxes of ^{210}Pb, ^{137}Cs and ^{241}Am determined from the soils of three small catchments in cumbria, UK. J. Environ. Radioact. 37 (2), 127–142. https://doi.org/10.1016/S0265-931X(97)00003-9.
Taieb Errahmani, D., Noureddine, A., Abril-Hernández, J.M., Boulahdid, M., 2020. Environmental radioactivity in a sediment core from Algiers Bay: radioecological assessment, radiometric dating and pollution records. Quat. Geochronol. 56, 101049. https://doi.org/10.1016/j.quageo.2019.101049.
UNESCO, 2021. Chréa Biosphere Reserve, Algeria. https://en.unesco.org/biosphere/arab-states/chrea. (Accessed October 2021).
Vidmar, T., 2005. Efftran - a Monte Carlo efficiency transfer code for gamma-ray spectrometry. Nucl. Instrum. Methods Phys. Res. 550, 603–608. https://doi.org/10.1016/j.nima.2005.05.055.
Wright, S.M., 2016. Predicted Caesium-137 deposition from atmospheric nuclear weapons tests. NERC Environmental Information Data Centre. https://doi.org/10.5285/c3e530bf-af20-43fc-8b4b-92682233ff08.
Zhang, F., Wang, J., Baskaran, M., Zhong, Q., Wang, Y., Paatero, J., Du1, J., 2021. A global dataset of atmospheric ^{7}Be and ^{210}Pb measurements: annual air concentration and depositional flux. Earth Syst. Sci. Data Discuss. https://doi.org/10.5194/essd-13-2963-2021.